Measurement depth and volume in laser Doppler flowmetry

Ingemar Fredriksson, Marcus Larsson and Tomas Strömberg

Original Publication:

Ingemar Fredriksson, Marcus Larsson and Tomas Strömberg, Measurement depth and volume in laser Doppler flowmetry, 2009, Microvascular Research, (78), 1, 4-13.
http://dx.doi.org/10.1016/j.mvr.2009.02.008

Measurement depth and volume in laser Doppler flowmetry

Ingemar Fredriksson
Marcus Larsson
Tomas Strömberg

Linköpings universitet
Department of Biomedical Engineering
University Hospital
S-581 85 Linköping
Sweden

Correspondence to:
Ingemar Fredriksson
Phone: 46 13 222483. Fax: 46 13 101902. E-mail: ingfr@imt.liu.se

Abstract: A new method for estimating the measurement depth and volume in laser Doppler flowmetry (LDF) is presented. The method is based on Monte Carlo simulations of light propagation in tissue. The contribution from each individual Doppler shift is calculated and thereby multiple Doppler shifts are handled correctly. Different LDF setups for both probe based (0.0, 0.25, 0.5, and 1.2 mm source-detector separation) and imaging systems (0.5 and 2.0 mm beam diameter) are considered, at the wavelengths 453 nm, 633 nm, and 780 nm. Non-linear speckle pattern effects are accounted for in the imaging system setups. The effects of tissue optical properties, blood concentration, and blood oxygen saturation are evaluated using both homogeneous tissue models and a layered skin model. The results show that the effect on the measurement depth of changing tissue properties is comparable to the effect of changing the system setup, e.g. source-detector separation and wavelength. Skin pigmentation was found to have a negligible effect on the measurement depth. Examples of measurement depths are (values are given for a probe based system with 0.25 mm source-detector separation and an imaging system with a 0.5 mm beam diameter, respectively, both operating at 780 nm): muscle – 0.55/0.79 mm; liver – 0.40/0.53 mm; gray matter – 0.48/0.68 mm; white matter – 0.20/0.20 mm; index finger pulp – 0.41/0.53 mm; forearm skin – 0.53/0.56 mm; heat provoked forearm skin – 0.66/0.67 mm.

Keywords: laser Doppler flowmetry; laser Doppler perfusion monitoring; laser Doppler perfusion imaging; source-detector separation; measurement volume; sampling depth; Monte Carlo simulations; tissue model; multiple Doppler shifts

1. Introduction

Laser Doppler Flowmetry (LDF) is an established method for measuring the microcirculatory blood flow using either a fiber optic probe (laser Doppler perfusion monitoring, LDPM) or an imaging system (laser Doppler perfusion imaging, LDPI). The technique is based on the Doppler frequency shift that occurs when monochromatic laser light is scattered by a moving object. In tissue, the fraction of Doppler shifted light depends on the concentration of moving red blood cells (RBC:s), whereas the magnitude of the frequency broadening depends on the average velocity of the RBC:s. In commercial LDF systems, these two microcirculatory quantities are monitored through a single perfusion value that under ideal conditions reflects the concentration of moving RBC:s times their average velocity. It can be shown that this value, given in arbitrary units, is linear to the average velocity, whereas it is non-linear to the concentration of RBC:s (Fredriksson, Fors *et al.* 2007). To improve the physiological interpretation of the measured quantities, it is necessary to predict the origin of the perfusion signal. Therefore, it is important to gain access to the measurement depth and/or volume, and how this depth/volume is affected by blood concentration, tissue type, and system setup.

Only a few authors have focused on this area before. The most cited article in the field is Jakobsson and Nilsson (1993), who investigated the median sampling depth for several probe geometries on liver, skin, and brain, using computer simulations based on the Monte Carlo technique. However, presumably due to the limited computational speed available in the early nineties, their tissue models were simple and they did not account for multiple Doppler shifts. Furthermore, additional knowledge on tissue optical properties is available today. Nilsson and Nilsson (1998) studied the influence of individual blood vessels in the superior and inferior vascular plexus in skin, concluding that more than 90 % of the detected photons were only affected by the superior plexus. However, as they also state, that does not imply that 90 % of the perfusion value originates from the superficial plexus as the average velocity is higher for the inferior plexus. Larsson, Steenbergen *et al.* (2002) investigated the effects on the optical path length and the sampling depth caused by the optical properties and the source-detector separation, using a sophisticated tissue phantom. It should be noted that the polystyrene spheres used as moving scatterers in that study scatters light much more diffusely than RBC:s, though. The sampling depth for an LDPI system has been briefly discussed by Rajan, Varghese *et al.* (2008), but they used a simplified tissue model with a single moving layer, as their main aim was to demonstrate how the complex effects of coherence areas affected the output from an LDPI system. Finally, Meglinsky and Matcher (2001) investigated the sampling volume of a spectroscopic system using a sophisticated skin model. However, their findings do not apply to LDF, since there is a fundamental difference in that the spectroscopy signal is based on tissue and blood absorption and not RBC scattering as in LDF.

As Jakobsson and Nilsson (1993), we make a difference between the sampling depth/volume and the measurement depth/volume. The sampling depth/volume only reveals where the detected photons have been propagating in the tissue, whereas the measurement depth/volume reveals the origin of the output signal. In LDF this is an important difference, as it is only blood that contributes to the perfusion value.

The aim of this article is to present typical measurement depths and volumes for the perfusion value for various types of tissue and system setups. This is achieved through Monte Carlo simulations of tissue relevant computer models where variations in tissue structure (single and multi layer), optical properties, blood amount and oxygen saturation, and system setup (including probe geometry, beam diameter, and wavelength), are evaluated.

2. Material and methods

2.1. Simulated system setups

The measurement depth and volume were investigated for three wavelengths: green light at 543 nm, used for a shallow depth (Tulevski, Ubbink *et al.* 1999); red light at 633 nm, the dominating wavelength used in older instruments and evaluated in the study by Jakobsson and Nilsson (1993); and near infrared light at 780 nm,

used in many modern laser Doppler perfusion monitors and employed in our previously presented skin model (Fredriksson, Larsson et al. 2008a).

Both fiber based LDF systems (LDPM) and imaging systems (LDPI) were investigated. LDPM systems with four different source-detector fiber separations were analyzed; 0.0 (single fiber), 0.25, 0.5, and 1.2 mm (center to center distance). All fibers had a core diameter of 0.125 mm and a numerical aperture of 0.37.

For the LDPI system, the tissue was illuminated with a uniform light beam with a diameter of either 0.5 or 2.0 mm. A light collecting lens with a diameter of 20 mm, focusing the backscattered light on the detector, was placed 200 mm above the tissue surface. All photons impinging the lens were used in the analysis.

2.2. Tissue models

The measurement depth and volume were investigated for several computer models; tissue specific homogeneous models (muscle, liver, and gray and white matter), a general homogenous model, and a layered skin model, all containing blood of various degrees. For the general homogeneous model, the effect of varying the optical properties (OP) of the static media (i.e. everything but the blood), the blood concentration, and blood oxygen saturation, was evaluated. For the static media, the absorption coefficient μ_a was varied between 0 and 10 mm^{-1}, the scattering coefficient μ_s was varied between 1 and 100 mm^{-1}, while the anisotropy factor $g = \langle\cos\theta\rangle$ (θ, scattering angle) was held constant at 0.85 giving a variation of the reduced scattering coefficient $\mu_s' = \mu_s(1 - g)$ between 0.15 and 15 mm^{-1}. The blood concentration was varied between 0.002 and 20 %, and the blood oxygen saturation was varied between 0 and 100 %. We defined a standard homogeneous tissue model with μ_a = 0.1 mm^{-1}, μ_s = 10 mm^{-1}, g = 0.85, and 0.2 % blood concentration with 80 % blood oxygen saturation.

For the tissue specific homogeneous models, e.g. muscle, liver, and gray and white matter, the OP:s are summarized in Table 1. In muscle tissue, absorption by static objects (i.e. not blood) was approximated with a 0.6 % myoglobin content (Jansson and Sylvén 1983) (assuming a 76.3 % water content in muscle (Bergstrom, Furst *et al.* 1974)), oxygenized to 90 % (Schenkman, Marble *et al.* 1999a). Myoglobin absorption data was compiled from Bowen (1949), Millar, Moss *et al.* (1996) and Shenkman, Marble *et al.* (1999b). Scattering data for muscle tissue was retrieved from Simpson, Kohl *et al.* (1998), using an $\alpha\lambda^{-\beta}$ (λ, wavelength) extrapolation for the shorter wavelengths, with a g = 0.90 assumption. The OP:s of liver was compiled from Ritz, Roggan *et al.* (2001) while the OP:s of gray and white matter were retrieved from Yaroslavsky, Schulze *et al.* (2002). We assumed a blood oxygen saturation of 80 % and a blood volume concentration of 1.0 % in muscle (van der Zee 1992), 20 % in liver (Taniguchi, Koyama *et al.* 1995), 4.5 % in gray matter, and 2.5 % in white matter (Hamberg, Hunter *et al.* 1996).

A recently developed skin model (Fredriksson, Larsson *et al.* 2008a), consisting of six layers, was also evaluated. Each layer was described by a standard thickness t and a standard blood concentration c_{blood} at three different blood flow velocities, as given in Table 2. Each velocity component had a uniform distribution of velocities, varying from 0 to twice the center velocity, at 0.3, 3.0, and 30 mm/s, respectively, with a random direction. The epidermis layer contained melanin but no blood, whereas the four dermis layers and the subcutis layer contained blood but no melanin. The standard OP:s of the layered skin model are summarized in Table 3. The effect of geometrical and blood flow related variations were evaluated by altering the overall thickness factor $f_{thickness}$ (scales all standard layer thicknesses equally and proportionally) and the overall blood concentration factors f_{blood} (scales the standard velocity components of a specific velocity in all layers equally and proportionally), were a factor of unity refers to the standard parameters. In addition, the effect of variations in melanin concentration has been evaluated in the interval 0 – 50 % melanin, representing white to black skin types (Jacques 1998). By pairing LDPM measurements with Monte Carlo simulations, tissue specific models of the unprovoked skin on the index finger pulp, and unprovoked and heat provoked skin of the volar side of the forearm, have been attained (Fredriksson, Larsson *et al.* 2008a). The parameters, i.e. the thickness factor and blood concentration factors, for these models are found in Table 4.

The OP:s of blood (hematocrit = 42 %) are summarized in Table 5. The scattering phase function for blood was modeled with a Gegenbauer kernel scattering phase function (Reynolds and McCormick 1980), with parameters α_{Gk} = 1.0 and g_{Gk} = 0.951, 0.950, and 0.948 for the wavelengths 543, 633, and 780 nm, respectively. The scattering phase functions for the static tissues were modeled with a Henyey-Greenstein phase function. The OP:s of blood, as well as the OP:s presented in Table 3, were compiled as described by Fredriksson, Larsson *et al.* (2008). In all models, the refractive index was set to 1.40 for all types of tissue to avoid Fresnel reflections between the unrealistically distinct and parallel borders between the layers in the skin model. Furthermore, the refractive index of the probe was set to 1.58 and the surrounding air to 1.00.

Table 1 Optical properties for muscle, liver, and gray and white matter.

	μ_a [mm^{-1}]			μ_s' [mm^{-1}]			μ_s [mm^{-1}]			g [-]		
Wavelength [nm]	**543**	**633**	**780**	**543**	**633**	**780**	**543**	**633**	**780**	**543**	**633**	**780**
Muscle	1.1	0.05	0.02	1.1	0.91	0.72	11	9.1	7.2	0.90	0.90	0.90
Liver	1.2	0.37	0.09	1.1	0.64	0.43	8.8	7.1	5.7	0.88	0.91	0.93
Gray matter	0.04	0.01	0.02	1.2	0.99	0.78	10	9.0	7.8	0.88	0.89	0.90
White matter	0.10	0.08	0.09	7.6	6.2	5.3	40	39	38	0.81	0.84	0.86

Table 2 Thickness and blood concentrations for the three velocity components for each layer in the standard skin model.

		c_{blood} [%]		
Layer	***t* [mm]**	**0.3 mm/s**	**3.0 mm/s**	**30 mm/s**
Epidermis	0.075	0	0	0
Papillary dermis	0.15	0.2	0	0
Superior blood net	0.15	0.6	0.05	0.001
Reticular dermis	0.80	0.1	0.01	0.0006
Inferior blood net	0.40	0.25	0.035	0.006
Subcutis	10	0.1	0.01	0.001

Table 3 Optical properties for (melaninless) epidermis, (bloodless) dermis, subcutis and melanin in the standard skin model.

	μ_a [mm^{-1}]			μ_s' [mm^{-1}]			μ_s [mm^{-1}]			g [-]		
Wavelength [nm]	**543**	**633**	**780**	**543**	**633**	**780**	**543**	**633**	**780**	**543**	**633**	**780**
Epidermis	0.25	0.15	0.10	5.8	4.8	3.5	39	32	23	0.85	0.85	0.85
Dermis	0.25	0.15	0.10	3.7	3.0	2.0	25	20	13	0.85	0.85	0.85
Subcutis	0.25	0.15	0.10	3.2	2.4	2.0	21	16	13	0.85	0.85	0.85
Melanin	51	30	15	-	-	-	-	-	-	-	-	-

Table 4 Thickness and blood concentration factors (multiplicative to the values in Table 2) for three specific skin model setups.

		f_{blood} [-]		
Tissue	$f_{thickness}$ **[-]**	**0.3 mm/s**	**3.0 mm/s**	**30 mm/s**
Unprovoked finger	1.8	1.9	17	270
Unprovoked forearm	0.95	0.34	0.80	1.9
Heat provoked forearm	1.4	1.4	18	75

Table 5 Optical properties for deoxygenated and oxygenated blood (hematocrit = 42 %).

	μ_a [mm^{-1}]			μ_s' [mm^{-1}]			μ_s [mm^{-1}]			g [-]		
Wavelength [nm]	**543**	**633**	**780**	**543**	**633**	**780**	**543**	**633**	**780**	**543**	**633**	**780**
Deoxygenated	30	2.7	0.64	2.34	2.13	2.00	292	237	222	.992	.991	.991
Oxygenated	38	0.34	0.50	2.34	2.13	2.00	292	237	222	.992	.991	.991

2.3. Monte Carlo simulations

The Monte Carlo technique, as applied in biomedical optics, uses stochastic sampling of probability distributions to simulate a large number of photon random walks, depending on the model geometry and scattering and absorption properties. Previous studies have demonstrated a high correlation between Monte Carlo based simulations and LDF measurements (de Mul, Koelink *et al.* 1995; Kienle, Patterson *et al.* 1996; Larsson, Steenbergen *et al.* 2002; Fredriksson, Larsson *et al.* 2006; Larsson and Strömberg 2006). In this study, an in-house Monte Carlo software (Fredriksson, Larsson *et al.* 2006; 2008a; 2008b) that tracks and stores information about each and every photon, including individual Doppler shifts, scattering positions, and photon weights, was used. When simulating the LDPI system, a forced detection variance reduction technique was applied to accelerate the simulations (Meier, Lee et al. 1978; Fredriksson, Larsson *et al.* 2008b). For both the LDPM and the LDPI simulations, the rotational symmetry of the tissue models was used to accelerate the simulations.

2.4. Data analysis

The LDF perfusion value increases with both the magnitude of the Doppler shifts (foremost dependent on the blood flow velocity) and the degree of Doppler shifted photons (dependent on the blood concentration). This needs to be accounted for when calculating the perfusion measurement depth or volume from a simulation. Consequently, for each detected photon, the signal contribution from each Doppler scattering event was calculated by taking into account the weight of the photon and the size of the Doppler shift in relation to all other Doppler shifts for that photon. Mathematically, this is expressed as

$$s_{m,n} = w_m \frac{\left|d_{m,n}\right|}{\sum_{k=1}^{K_m}\left|d_{m,k}\right|}\left|\sum_{k=1}^{K_m} d_{m,k}\right| \qquad (1)$$

where $s_{m,n}$ is the signal contribution from the n:th Doppler scattering event of photon m, w_m is the weight of the detected and Doppler shifted photon, $d_{m,n}$ is the size of the Doppler shift n, K_m is the total number of Doppler shifts for photon m, and $|\ldots|$ expresses the absolute value. Note that some Doppler shifts have a positive sign and some a negative.

The measurement depth/radius was determined such that the sum of the signal contributions located above/within this depth/radius accounted for $1 - e^{-1} \approx 63$ % of the sum of all signal contributions. The measurement volume was calculated as the volume of a half sphere with the determined radius. A depth of zero corresponded to the surface of the model. The center of the sphere was positioned either in the middle between the emitting and detecting fiber tip (for the LDPM setups) or in the center where the laser beam impinged the tissue (for the LDPI setups).

Due to non-linear speckle effects, affecting the measurement depth and volume for the LDPI setups, the photon weights were adjusted before used in equation 1. The adjustment was only applied to LDPI data where the intensity varies between coherence areas. This effectively increased the impact of photons being backscattered from the tissue close to the area of illumination, and is further described in the Appendix.

In Figure 1, an example of the spatial distribution of the signal contribution ($s_{m,n}$) can be seen, both in a projection from aside and a projection from above. The measurement depth (0.39 mm) and volume (0.23 mm^3, radius 0.48 mm) are marked with the dashed black lines. The emitting and receiving fibers are also marked. In Figure 2, the signal contribution as a function of depth, as well as its cumulative sum, is shown. The level $1 - e^{-1}$ is reached at the depth 0.39 mm. This example is from the standard homogeneous model at 780 nm (compare with Table 6).

For comparison, the data analysis described by Jakobsson and Nilsson (1993) was evaluated for selected models.

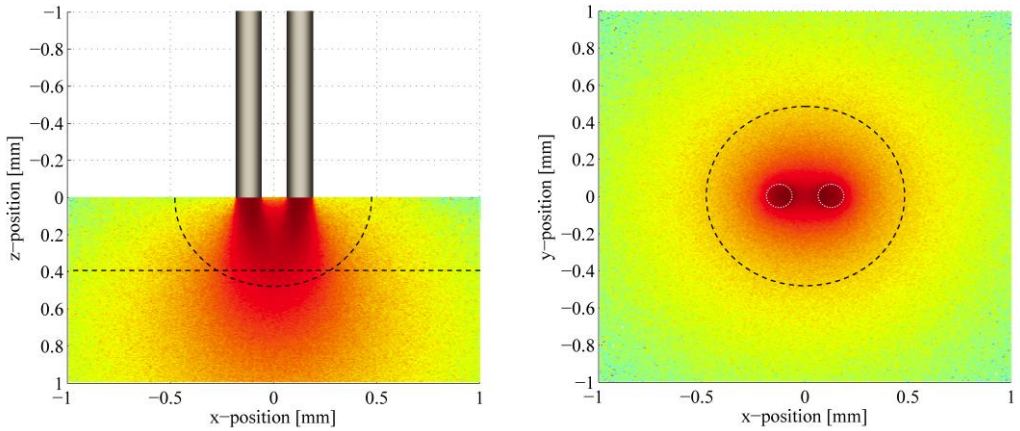

Figure 1 Example of the signal contribution from each position. The intensity scale is logarithmic.

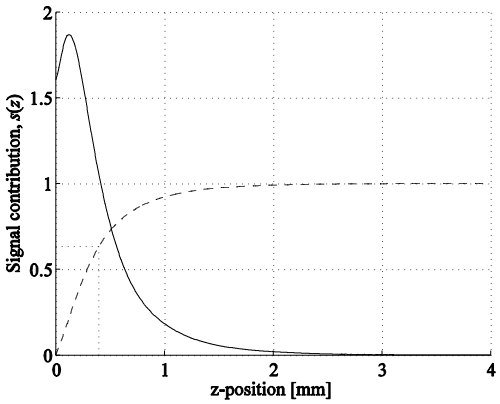

Figure 2 Example of the signal contribution (solid line) and the cumulative sum of the signal contribution (dashed line), both as a function of depth. The marked cumulative level $1 - e^{-1}$ is reached at the depth 0.39 mm.

3. Results and discussion

3.1. Homogeneous model

The measurement depth and volume are given in Table 6 for the standard homogenous tissue model (μ_a = 0.1 mm^{-1}, μ_s = 10 mm^{-1}, g = 0.85, 0.2 % blood, 80 % blood oxygen saturation). Both the measurement depth and volume increase with the source-detector separation, which is expected. The increase is more rapid in the measurement volume since the volume is proportional to the radius cubed.

The depth and volume also increase when the beam diameter in the LDPI system increases, which is intuitive for the volume, but may be surprising for the depth. For an LDPI system, most of the backscattered light escapes the tissue close to the area of injection. It is these photons that will have the main impact on the perfusion signal, as stated previously. However, as the beam diameter increases, the probability of propagating longer and deeper into the tissue, while still being able to escape close to the injection area, increases. As a result, both the measurement depth and volume will increase with the beam diameter.

Another observation in Table 6 is that the measurement depth and volume increase with wavelength. This is because the light absorption of blood decreases with wavelength for these three wavelengths. It is however not a general trend that the blood absorption decreases with wavelength (Zijlstra, Buursma *et al.* 2000).

Table 6 Measurement depth and volume for the standard homogeneous model.

LDPM fiber sep. / LDPI beam ∅		Measurement depth [mm]			Measurement volume [mm^3]		
		543 nm	633 nm	780 nm	543 nm	633 nm	780 nm
LDPM	0.0	0.15	0.17	0.17	0.012	0.015	0.016
LDPM	0.25	0.36	0.39	0.39	0.16	0.23	0.23
LDPM	0.50	0.45	0.49	0.50	0.39	0.55	0.56
LDPM	1.2	0.61	0.67	0.67	1.4	1.9	2.0
LDPI	0.5	0.41	0.47	0.48	0.63	1.1	1.2
LDPI	2.0	0.50	0.57	0.58	2.3	3.1	3.2

Figures 3-6 present the changes in measurement depth relative to the values in Table 6, when one (open symbols) or more parameters (closed symbols) in the tissue model are changed. Only data for the source-detector separation 0.25 mm are presented. The other source-detector separations and the LDPI setups generally follow the same trends. The volume also follows the same trends, although it is affected even stronger.

In general, the measurement depth/volume is inversely related to the level of absorption. This is explained by the fact that an increase in absorption coefficient mainly will decrease the amount of long-path-length photons, effectively decreasing the measurement depth/volume. Because the absorption coefficient of blood is generally higher than for the surrounding tissue, it is expected that the measurement depth and volume decrease when the blood concentration increases. This can be seen in Figure 3 (open symbols). When the absorption of the surrounding medium is high (μ_a = 10 mm^{-1} for the closed symbols as compared to 0.1 mm^{-1} for the open symbols), this effect is smaller and the depth is much more shallow. Then, the absorption of the surrounding medium is even higher than the absorption of blood at 633 and 780 nm, which is the reason that the measurement depth and volume increase slightly with high blood concentration at these wavelengths.

In addition, the increased blood concentration also increases the degree of multiple Doppler shifted photons. The degree of multiple Doppler shifts is relatively higher for photons having propagated a long distance, and therefore their contribution to the perfusion signal will scale nonlinearly to the blood concentration and the measurement depth and volume will decrease compared to a lower blood concentration. This is the main reason why the measurement depth is affected even by changes at very low blood concentrations in the standard model.

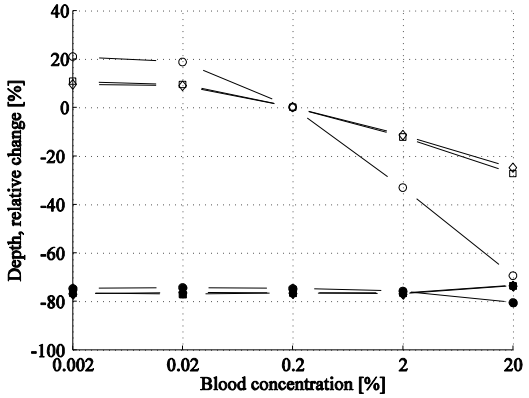

Figure 3 Change of measurement depth in the standard homogenous tissue model, when only the blood concentration changes (open symbols), and when the blood concentration changes while the absorption coefficient of surrounding medium μ_a = 10 mm^{-1} (closed symbols). Circles – 543 nm, squares – 633 nm, diamonds – 780 nm.

The absorption coefficient is not the same for oxygenated and deoxygenated blood (Table 5). Therefore, it is expected that the measurement depth/volume is affected when the oxygenation status of the blood changes. It can be seen in Figure 4 that this effect is very small for the standard properties of the homogenous model (open symbols), but when the blood concentration is extremely high, c_{blood} = 20 %, in combination with a low absorption and scattering of the surrounding medium, μ_a = 0.0 mm^{-1}, μ_s' = 0.15 mm^{-1}, there is a

significant change (closed symbols). This change is most prominent at 633 nm, where the difference in the absorption coefficient of oxygenated and deoxygenated blood is large.

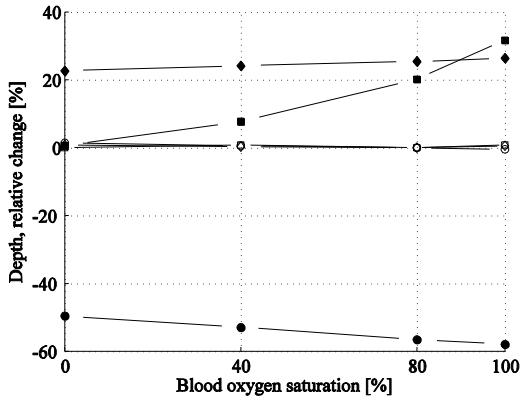

Figure 4 Change of measurement depth in the standard homogenous tissue model, when only the blood oxygen status changes (open symbols), and when the blood oxygen status changes while c_{blood} *= 20 %,* μ_a *= 0.0 mm*$^{-1}$*,* μ_s' *= 0.15 mm*$^{-1}$ *of the surrounding medium (closed symbols). Circles – 543 nm, squares – 633 nm, diamonds – 780 nm.*

As observed in Figure 3, and separately studied in Figure 5, the measurement depth decreases when the absorption coefficient of the surrounding medium increases. This effect is relatively small at 543 nm, due to the high absorption coefficient of blood. Furthermore, the effect is smaller when the blood concentration is high (c_{blood} = 20 %, closed symbols).

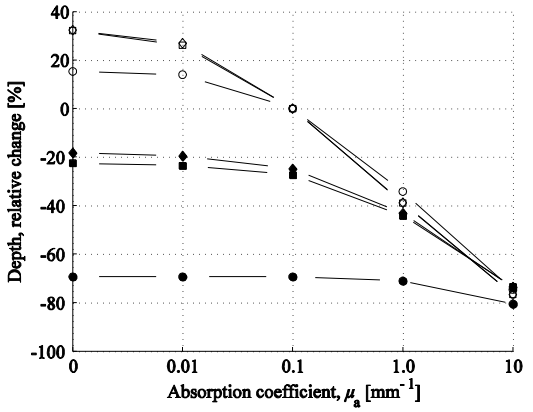

Figure 5 Change of measurement depth in the standard homogenous tissue model, when only the absorption coefficient of the surrounding medium changes, and when the absorption coefficient of the surrounding medium changes, while c_{blood} *= 20 % (closed symbols). Circles – 543 nm, squares – 633 nm, diamonds – 780 nm.*

When the scattering coefficient increases, the propagation depth of the photons will decrease, which can be seen in Figure 6. When the concentration of blood is low, this will affect all three wavelengths almost identically since the average OP:s are almost identical, but when the concentration of blood is high (c_{blood} = 20 %, closed symbols), the effect will be greater at 543 nm since the blood absorption is significantly higher at this wavelength than at the other two.

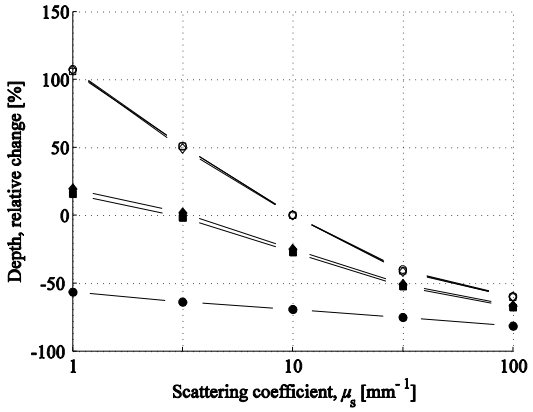

Figure 6 Change of measurement depth the standard homogenous tissue model, when the scattering coefficient of the surrounding medium changes. Closed symbols – c_{blood} = 20 %. Circles – 543 nm, squares – 633 nm, diamonds – 780 nm.

The measurement depths and volumes for the tissue models for muscle, liver, and gray and white matter (Table 1) are presented in Table 7 and Table 8, respectively. The smallest measurement depths are found for liver and white matter. For liver, the small measurement depth is due to a very high absorption and blood concentration, whereas the small measurement depth in white matter is foremost due to a very high scattering.

Table 7 Measurement depth in mm for the tissue models of muscle, liver, and gray and white matter.

LDPM fiber sep. /		Muscle			Liver			Gray matter			White matter		
LDPI beam ∅		543	633	780	543	633	780	543	633	780	543	633	780
LDPM	0.0	.10	.18	.19	.046	.11	.13	.088	.15	.16	.064	.092	.099
LDPM	0.25	.23	.48	.55	.11	.31	.40	.21	.43	.48	.12	.19	.20
LDPM	0.50	.29	.62	.73	.14	.40	.52	.27	.58	.64	.17	.27	.28
LDPM	1.2	.40	.83	.96	.19	.56	.71	.37	.79	.86	.26	.45	.46
LDPI	0.5	.19	.60	.79	.053	.23	.53	.17	.48	.68	.10	.17	.20
LDPI	2.0	.24	.73	.92	.054	.32	.66	.21	.59	.81	.12	.22	.26

Table 8 Measurement volume in mm^3 for the tissue models of muscle, liver, and gray and white matter.

LDPM fiber sep. /		Muscle			Liver			Gray matter			White matter		
LDPI beam ∅		543	633	780	543	633	780	543	633	780	543	633	780
LDPM	0.0	.003	.016	.020	.001	.004	.006	.003	.010	.012	.001	.004	.004
LDPM	0.25	.038	.34	.51	.008	.084	.17	.030	.26	.32	.013	.036	.041
LDPM	0.50	.10	.90	1.4	.033	.21	.45	.084	.75	.93	.048	.14	.15
LDPM	1.2	.55	3.0	4.3	.29	.89	1.6	.52	2.8	3.2	.37	.88	.92
LDPI	0.5	.046	2.0	4.6	.016	.079	1.2	.041	.98	3.2	.028	.089	.13
LDPI	2.0	1.0	5.1	9.0	.97	1.2	3.6	1.0	3.2	6.8	.87	1.1	1.3

3.2. Skin model

The measurement depth and volume for the skin model presented in Tables 2-3, are given in Table 9. Due to the bloodless epidermis layer the measurement depth changes less in this model than in the homogeneous model when the source-detector separation increases. As for the homogeneous model, the measurement depth and volume increase with wavelength. In this case, this is not only due to the variations in absorption by blood, but also that both the absorption and scattering decrease with wavelength for dermis and subcutis tissue, see Table 3.

Table 9 Measurement depth and volume for standard skin model setup.

LDPM fiber sep. / LDPI beam ∅		Measurement depth [mm]			Measurement volume [mm^3]		
		543 nm	633 nm	780 nm	543 nm	633 nm	780 nm
LDPM	0.0	0.28	0.30	0.32	0.076	0.096	0.11
LDPM	0.25	0.30	0.32	0.35	0.10	0.14	0.19
LDPM	0.50	0.31	0.34	0.37	0.16	0.23	0.38
LDPM	1.2	0.36	0.40	0.58	0.65	0.99	1.9
LDPI	0.5	0.30	0.33	0.37	0.17	0.33	0.84
LDPI	2.0	0.32	0.35	0.44	1.2	1.7	2.9

The changes in measurement depth relative to the values in Table 9, when the thickness factor $f_{\text{thickness}}$ and the various blood velocity component factors f_{blood} are changed, for the source-detector separation 0.25 mm, are given below. When the thickness factor increases, the measurement depth generally increases, which can be seen in Figure 7. This is mainly due to the increased thickness of the bloodless epidermis layer. The influence of the thickness of the other layers is more difficult to predict and follows no general trends. The reason that the measurement depth may decrease with increased thickness factor is that deeper, blood rich, layers reduce their influence as they become too deep.

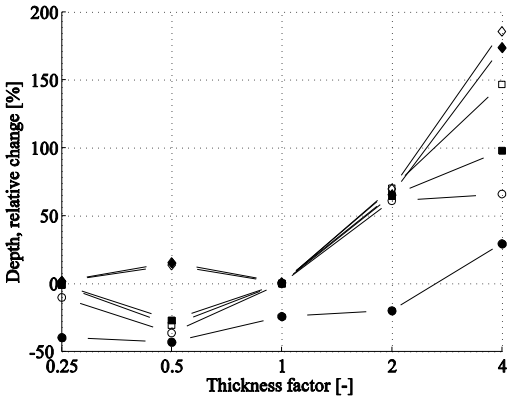

Figure 7 Change in measurement depth for the standard skin model and a source-detector separation 0.25 mm, when only the thickness factor is changed (open symbols), and when the thickness factor is changed while all blood velocity components increased by a factor of 16 (closed symbols). Circles – 543 nm, squares – 633 nm, diamonds – 780 nm.

Various effects take place when the blood concentrations in the layered skin model change. First, since the absorption coefficient of blood is higher than for the surrounding medium, the measurement depth decreases due to the higher total absorption when the blood concentration increases. As discussed at Figure 3, the measurement depth also decreases due to the higher degree of multiple Doppler shifts for deep propagating photons when the blood concentration increases. On the other hand, since the blood concentration varies considerably between the layers, a deeper layer can have a higher impact when the blood concentration increases, which leads to an increased measurement depth. These effects can be observed in Figure 8. It is especially interesting to study the highest velocity component (30 mm/s), which has a relative high concentration in the deeper layers. There it can be seen that the measurement depth initially increases when the concentration of that component increases, due to the higher impact from the deeper layers, but when the concentration increases even more, the absorption effect and effect of multiple Doppler shifts become dominating and the measurement depth decreases.

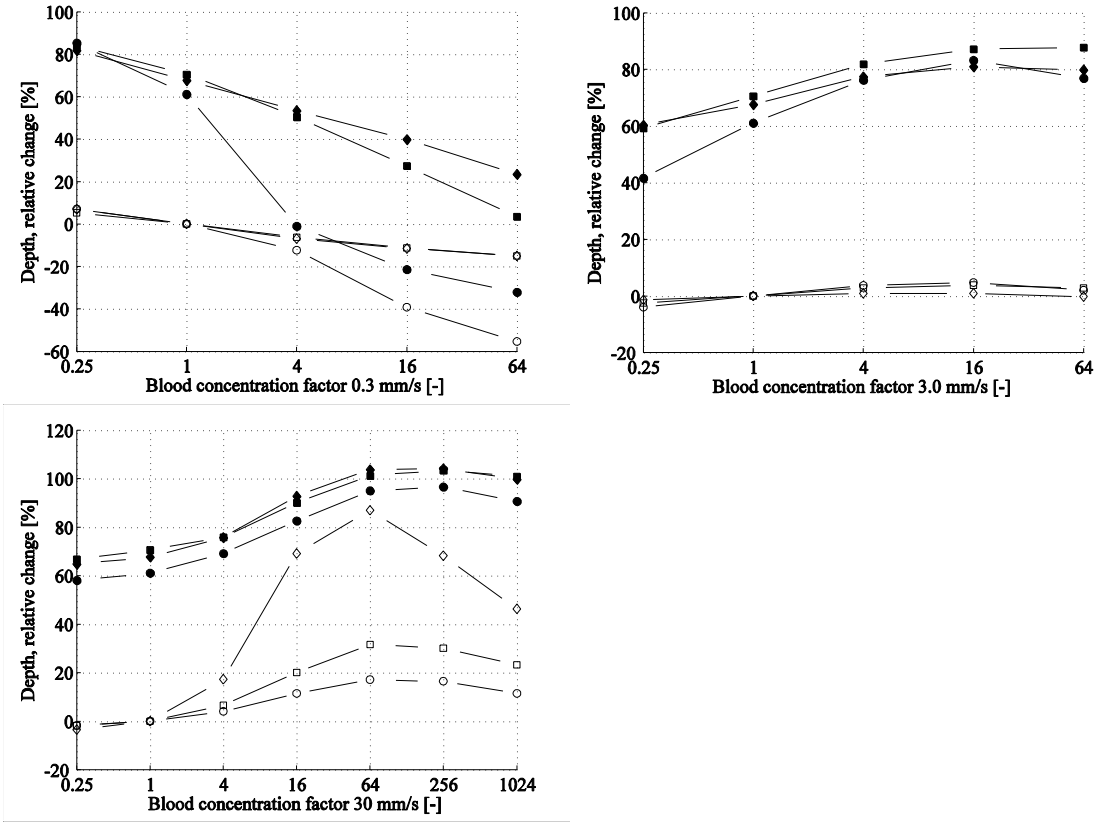

Figure 8 Change in measurement depth in the standard skin model for source-detector separation 0.25 mm when only the blood concentration for the three blood flow velocities is changed (open symbols), and when the concentrations are changed while the layer thickness is increased by a factor 2 (closed symbols). Circles – 543 nm, squares – 633 nm, diamonds – 780 nm.

The effect of the melanin concentration in epidermis on measurement depth showed a change less than 4 % when the melanin concentration was changed between 0 and 50 %, i.e. between white and black skin types. A maximal effect was observed at 543 nm, where the measurement depth increased slightly (4 %) with melanin concentration for the largest source-detector separation, and decreased slightly (2 %) for the closest separation.

The measurement depth for the skin models in Table 4 are presented in Table 10 and the measurement volume in Table 11. It is especially interesting to study the difference between unprovoked and heat provoked forearm skin. An intuitive assumption may be that the measurement depth/volume would decrease during the provocation due to the increased blood volume. These findings, however, show that the effect is the opposite since the blood concentration in the deeper blood vessels with higher blood flow velocity increases the most, leading to a higher contribution from greater depths. An in-depth discussion about the skin models have been presented by Fredriksson, Larsson *et al.* (2008).

Table 10 Measurement depth in mm for the three specific skin models as in Table 4.

LDPM fiber sep. /		Index finger			Forearm unprovoked			Forearm provoked		
LDPI beam ∅		543 nm	633 nm	780 nm	543 nm	633 nm	780 nm	543 nm	633 nm	780 nm
LDPM	0.0	0.31	0.33	0.35	0.43	0.48	0.52	0.52	0.60	0.65
LDPM	0.25	0.32	0.35	0.41	0.44	0.49	0.53	0.53	0.61	0.66
LDPM	0.50	0.34	0.36	0.50	0.45	0.50	0.55	0.54	0.61	0.67
LDPM	1.2	0.40	0.53	0.85	0.50	0.56	0.70	0.58	0.66	0.73
LDPI	0.5	0.33	0.36	0.53	0.44	0.50	0.56	0.53	0.62	0.67
LDPI	2.0	0.34	0.39	0.68	0.46	0.52	0.63	0.55	0.64	0.70

Table 11 Measurement volume in mm^3 for the three specific skin models as in Table 4.

LDPM fiber sep. / LDPI beam ∅		Index finger			Forearm unprovoked			Forearm provoked		
		543 nm	633 nm	780 nm	543 nm	633 nm	780 nm	543 nm	633 nm	780 nm
LDPM	0.0	0.11	0.13	0.17	0.28	0.47	0.68	0.47	0.88	1.2
LDPM	0.25	0.14	0.21	0.42	0.30	0.51	0.75	0.51	0.91	1.3
LDPM	0.50	0.22	0.34	0.80	0.36	0.62	1.0	0.57	1.0	1.5
LDPM	1.2	0.81	1.5	4.1	0.82	1.5	2.6	1.0	1.8	2.7
LDPI	0.5	0.25	0.50	2.0	0.40	0.80	1.7	0.60	1.3	2.2
LDPI	2.0	1.4	2.1	5.0	1.5	2.3	4.0	1.7	2.8	4.3

3.3. Comparison with previous study

A comparison with the analysis method presented by Jakobsson and Nilsson (1993) has been carried out. Table 12 shows the measurement depth for various blood concentrations for the homogeneous model with $\mu_a = 0.1$ mm^{-1}, $\mu_s = 10$ mm^{-1}, $g = 0.85$, 80 % blood oxygen saturation, at 633 nm. In the Jakobsson and Nilsson method, a homogeneous perfusion distribution was used to achieve the measurement depth. Beside the limit of $1 - e^{-1}$ that has been used throughout this article, an additional limit of 0.5, which corresponds to the median measurement depth estimated in the Jakobsson and Nilsson method, has been used for the new method. The limit 0.5 reduces the measurement depth by 25-30 % as compared to the depths estimated using the limit $1 - e^{-1}$.

The values in Table 12 can be compared to Figure 3. The measurement depth decreases with blood concentration due to the high absorption coefficient of blood. This is the only reason that the measurement depth calculated with the Jakobsson and Nilsson method decreases at high blood concentrations. However, there is a second effect that causes the measurement depth to decrease with blood concentration – the increased degree of multiple Doppler shifted photons when the blood concentration increases. This is not accounted for in the Jakobsson Nilsson method and the difference is evident when comparing the changes in measurement depth for low blood concentrations between the two methods. Furthermore, the new method accounts for the increase in measurement depth with beam diameter in an LDPI system (Table 6), which is not accounted for in the Jakobsson and Nilsson method (not shown in Table 12).

Table 12 Comparison of measurement depth calculated with the new method in this paper and with the method presented by Jakobsson and Nilsson (1993), for the standard homogeneous tissue model with blood concentration ranging from 0.002 to 20 %. For the new method, both the limit $1 - e^{-1}$ used throughout this article, and the limit 0.5 which offers a better comparison to the Jakobsson and Nilsson method, were employed.

	LDPM fiber sep. / LDPI beam ∅		Measurement depth [mm]				
			0.002 %	0.02 %	0.2 %	2 %	20 %
Jakobsson & Nilsson	LDPM	0.25	0.27	0.27	0.27	0.26	0.22
	LDPI	0.5	0.53	0.52	0.52	0.50	0.37
New method, 0.5	LDPM	0.25	0.31	0.31	0.29	0.25	0.21
	LDPI	0.5	0.40	0.38	0.34	0.29	0.21
New method, $1 - e^{-1}$	LDPM	0.25	0.43	0.43	0.39	0.34	0.28
	LDPI	0.5	0.55	0.54	0.47	0.41	0.30

3.4. Methodological discussion

The presented method is unique as it is based on the position and size of each individual Doppler shift, rather than estimating the measurement depth from the sampling depth. This is the only way that multiple Doppler shifts can be accounted for correctly, suppressing the contribution from photons that have been propagating deep into the tissue. It must be stressed that the measurement depth/volume given is valid for the perfusion value only, and not to the CMBC value (concentration of moving RBC:s) as this value does not depend on the size of each Doppler shift. Hence, the measurement depth for the CMBC will likely be shallower than for the perfusion, also for the homogeneous models.

The important difference between measurement depth and sampling depth can be realized by considering skin tissue. The top layer in skin, epidermis, contains no blood. However, if the epidermis is thick, most photons may not reach deeper than the epidermis and thus the sampling depth would be no deeper than epidermis. Because the LDF-signal is generated by Doppler shifts caused by moving RBC:s, there would be no LDF-signal from within the sampling depth in this case. Therefore, the sampling depth is not as important as the measurement depth in LDF applications.

We have set the limit of the measurement depth to $1 - e^{-1}$, which means that the major part of the contribution ($1 - e^{-1} \approx 63$ %) to the perfusion signal originates from above this depth. The limit is motivated by assuming an exponential decay in signal contribution (see Figure 2) and is often used when expressing light penetration in tissue. In (Jakobsson and Nilsson 1993), the median measurement depth was estimated, which corresponds to the limit of 0.5. As mentioned in section 3.3, the difference in measurement depth using these two limits was 25-30 %, for the model and system setups evaluated there.

The estimation of the measurement volume is similar to the estimation of the depth, with the only difference that the depth is replaced by a half sphere. The decision of representing the volume as a half sphere may be questioned, though. It can for example be seen in Figure 1 that the half sphere is not a very good representation of the geometry where the signal contribution is the highest. Although the half sphere is a better representation in other situations, for example for longer source-detector separations, it may also be a much worse representation in other cases. One extreme case is liver with the 2.0 mm beam diameter LDPI setup at 543 nm. As can be seen in Table 7, the measurement depth is very shallow in this case due to the high absorbance in the tissue, but the estimated measurement volume is relatively large since the signal contribution is high in a wide but shallow layer just beneath the tissue surface. The reason that we have chosen the half sphere geometry despite these problems is that it is an intuitive geometry and represents the actual geometry rather well in many situations.

Measurement depths and volumes for both LDPM setups with various source-detector separations, and LDPI setups with various beam diameters, have been presented. When using an LDPM system with a long source-detector separation, it is common to place several detector fibers in a circle around the source fiber. This alternative design has no impact on the measurement depth, but the measured volume will obviously increase. The measurement volume generally increases by 60-100 % with this alternative design, placing the center of the half sphere in the center of the source fiber.

In the case of LDPI, the method takes into account the number of active coherence areas. The effect of this has also been discussed. The theory is based on an LDPI system with a light collecting lens in front of the photo detector. Rajan, Varghese *et al.* (2006) have shown that the effect is identical in a system without a lens, under the assumption that the spot on the tissue surface from which backscattered photons illuminate the detector, has a homogeneous intensity distribution. Although it has not been shown that this holds for the general case with an inhomogeneous spot, there are reasons to believe that the effect is at least similar in such a system, and the results presented here can be adopted also for a system without a lens.

The results presented for LDPI are valid when no specularly reflected light hits the detector. When specular reflections impinge the detector to a significant degree, the total detected light intensity (the dc-level) will increase and the fraction of Doppler shifted photons will thus decrease, resulting in a lowered perfusion value (for a dc^2-normalized system). Specular reflections will also decrease the measurement depth and volume since the specularly reflected light will increase the impact from photons that are diffusely back scattered at the illumination point where the intensity is the highest (see the Appendix). These photons have generally not been deep into the tissue, and therefore the measurement depth and volume will decrease. Consequently, for example the melanin concentration can affect the measurement depth and volume to some extent since the fraction of the detected light that is specularly reflected will increase for darker skin types when the diffusely backscattered light is decreased due to tissue absorption.

Others have presented various hardware approaches that enable depth discrimination in LDF measurements. The most popular methods use different wavelengths (Koelink, De Mul *et al.* 1994; Tulevski, Ubbink *et al.* 1999) or different source-detector separations (Larsson, Steenbergen *et al.* 2002). This study does not only show that changing the wavelength and/or source-detector separation has a major impact on the measurement depth, but also that changing tissue properties within relevant intervals has an effect on the measurement depth that is comparable with changing the system setup.

3.5. Implications on *in vivo* measurements

For LDPI systems and LDF probes with a fiber separation < 1.2 mm, skin surface measurements depths are well within the dermal layers, including only capillaries, arterioles, and venules (the microcirculation). The

macrocirculatory arteries and veins are found in the deeper lying subcutis and are therefore generally not affecting the LDF measurements. However, due to the size and blood velocity of arteries and veins, it is likely that they can affect the measurement when situated superficially in the subcutis just beneath the measurement site. This can sometimes be seen in images from LDPI measurements (Arildsson, Wårdell *et. al.* 1997; Serov and Lasser 2006).

As for muscle, brain and liver tissues, LDPI measurements are done on the surface, while LDPM measurements may either be on the surface or within the tissue using a needle probe. In skeletal muscles, arteries branch into arterioles at regular intervals of about 1 mm. The arterioles usually run orthogonal to the muscle fibers, whereas the high amount of capillaries that branch from the arterioles run parallel to the muscle fibers. The capillaries are collected into venules which run between the arterioles, and the venules finally unite into veins which follow the arteries. The distance between pairs of arteries and veins is several mm, whereas the distance between arterioles and venules is only in the order of 0.5 mm. The microvascular network in the muscle (arterioles, capillaries, and venules) is thus approximately homogeneous in comparison with the measurement volumes given for most fiber separations and wavelengths for muscle in Table 8. If a probe is positioned close to an artery-vein-pair, the LDF measurement will be affected and the homogeneous model assumption will be incorrect, though.

Most of the large arteries and veins in the brain are located on the brain surface and quickly branch within the brain. Therefore, intracerebral measurement on both gray and white matter can be considered to originate from a homogeneous distribution of microvascular vessels on the scale of the measurement volumes given in Table 8 at most fiber separations and wavelengths. However, as for muscle tissue, this is not true when measuring close to the arteries and veins at the surface of the brain or any of their large branches within the brain.

The liver consists of small (a few mm^3 large) lobules. A central vein is located in the center of each lobule, and portal vein branches are located between the lobules, accompanied by small arteries. The central vein and the portal vein branches have a diameter in the order of 100 µm, and the arteries are somewhat smaller. A large amount of small vessels (~30 µm), called sinusoids, connect the portal vein branches and the central veins. The two types of veins are relatively homogeneously distributed with separations in the order of 0.5 mm. Due to the small measurement volume in liver for small fiber separations especially at 543 nm, the measured quantity may be strongly dependent on the exact position of the probe within the lobule, whereas the larger measurement volumes for the other wavelengths and larger fiber separations justify the homogeneous model of the liver.

The tissue models presented in this article are based on best available knowledge on anatomical and optical properties, but are nevertheless only generalized models. To reveal the actual measurement depth/volume in a specific measurement site on a specific subject, the model has to be individualized. We have previously suggested a method applicable to skin, where the layer thicknesses and blood concentrations in three different flow velocities in the model were estimated based on LDF measurements at two different source-detector separations (Fredriksson, Larsson *et al.* 2008a). This method is suitable to individualize the skin model to predict the measurement depth/volume, and was used to estimate the model parameters in the specific skin models in Table 4.

4. Conclusions

We have developed a new method for estimating the measurement depth and volume in laser Doppler flowmetry, based on the Doppler scattering events during random walks of photons simulated with the Monte Carlo technique. The most important previous study in the topic was based on the distributions of the maximal photon depth weighted by the red blood cell distribution (Jakobsson and Nilsson 1993). The new method takes multiple Doppler shifts into account, which is an important improvement. The new method also handles non-intuitive speckle effects in LDPI. The method was used for evaluating homogenous tissue models, and a multilayer skin model. The effect of varying the properties of the models was studied in detail, and examples of measurement depth and volumes for models representing muscle, liver, brain, and various skin types have been presented. It was concluded that skin pigmentation had a negligible effect on the measurement depth. The measurement depth was less than 1.0 mm for all evaluated models and system setups.

5. Acknowledgements

The project was supported by the NIMED Center for Biomedical Data Processing, where this project was funded by Linköping University and Perimed AB.

Appendix

In an LDF system, the estimated perfusion scales with the frequency content and the magnitude of the time varying part of the photo detector current i_{ac}, normalized with the average total detector current i_{dc} squared. The variation in i_{ac} is expressed as the variance $\langle i_{ac}^2 \rangle$. For each coherence area i on the detector, this variation can be calculated from the fraction of Doppler shifted photons f_i impinging the coherence area (Serov, Steenbergen *et al.* 2001) as

$$\langle i_{ac}^2 \rangle_i = \langle i_{dc} \rangle_i^2 f_i(2 - f_i), \qquad (2)$$

where $\langle i_{dc} \rangle_i$ is the average detector current generated by coherence area i. The values of f_i and $\langle i_{dc} \rangle_i$ are given from the simulations as the fraction of Doppler shifted photons and the total amount of photons, respectively, impinging coherence area i.

The stochastic nature of the speckle pattern implies that each speckle (i.e. coherence area) can be treated as an independent stochastic process. As a consequence, the variance of the total detected signal can be expressed as

$$\langle i_{ac}^2 \rangle = \sum_{i=1}^{A} \langle i_{ac}^2 \rangle_i \qquad (3)$$

where A is the number of coherence areas.

From equations 2 and 3 it can be realized that the magnitude of $\langle i_{ac}^2 \rangle$ and hence the perfusion value will scale inversely to the number of coherence areas, for the same amount of light and fraction of Doppler shifted light that impinges the detector. When analyzing the LDPI simulations, the detector surface was divided into A equally sized bins, each representing one coherence area. Each photon was assigned to a single bin according to its position of detection. The size of A was chosen sufficiently large to ensure that the spatial intensity distribution within each bin was approximately constant, but not too large to avoid stochastic fluctuations due to the limited number of simulated photons. This ensures that the measurement depth and volume are independent of A. For each bin, $\langle i_{ac}^2 \rangle_i$ was calculated according to equation 2. According to that equation, the intensity $\langle i_{dc} \rangle_i$ in each coherence area does not linearly contribute to $\langle i_{ac}^2 \rangle_i$, and therefore not linearly to $\langle i_{ac}^2 \rangle$ (equation 3) and the perfusion value. Consequently, when the intensity varies over the detector, as in an LDPI setup using an imaging lens system (see below), each photon weight, which contributes linearly to the light intensity $\langle i_{dc} \rangle_i$, will not contribute linearly to the *signal contribution* in equation 1. Therefore, to make equation 1 valid for an LDPI setup the weight of each photon has to be adjusted. The weight adjustment was set to fulfill

$$\begin{cases} \sum_{j \in D_i} w'_{i,j} = \langle i_{ac}^2 \rangle_i \\ w'_{i,j} = k_i w_{i,j} \end{cases}, \qquad (4)$$

where $w'_{i,j}$ is the adjusted photon weight of Doppler shifted photon j in coherence area i, D_i is the Doppler shifted photons in that coherence area, and k_i the weight adjusting coefficient for the photons in coherence area i. This implies that the sum of the reweighted photons in coherence area i is forced to equal $\langle i_{ac}^2 \rangle_i$, and all photons within one coherence area are reweighted with the same factor. Thus, the weight of every Doppler shifted photon was adjusted according to

$$w'_{i,j} = \langle i_{ac}^2 \rangle_i w_{i,j} \Big/ \sum_{j \in D_i} w_{i,j}, \qquad (5)$$

where $w_{i,j}$ is the original photon weight. The adjusted photon weight $w'_{i,j}$ was used in equation 1 to calculate the signal contribution from a single photon in the LDPI setups.

In an LDPM system, all coherence areas have equal intensity and a constant size, depending only on the fiber-detector properties and not the tissue optical properties (i.e. the number of coherence areas is hardware

dependent only) (Serov, Steenbergen *et al.* 2001). Therefore, the weight adjustment in equation 5 is identical for all photons and the measurement depth and volume are not affected by it. Consequently, the weight adjustment was not performed in the analysis of the LDPM simulations.

For an LDPI system without a light collecting lens in front of the detector, the size, and therefore the number of the coherence areas that fit on the detector, depends on the solid angle of the light impinging the detector. For an LDPI system with a lens that focuses the backscattered light on the detector (i.e. imaging optics), the solid angle is solely determined from the lens configuration. Assuming a fixed lens configuration, the size of each coherence area will be constant. However, due to the imaging optics, where the detector is positioned in focus, the intensity of each coherence area will depend on the spatial distribution of the backscattered photons, affecting the number of active coherence areas (Rajan, Varghese *et al.* 2006). For both types of systems, the detected Doppler signal will similarly depend on the size of the surface area where the backscattered photons escapes the tissue, either influencing the magnitude of the solid angle (non-lens setup) or the number of active coherence areas (lens setup). The calculated perfusion value will have an inverse relationship to the spot size, with a main contribution from photons escaping the tissue within or close to the area of illumination where the backscattered intensity is the highest. These speckle size/intensity related effects were accounted for in the LDPI analysis with the weight adjustment in equation 5.

References

Arildsson, M. L., Wårdell, K. and Nilsson, G. E., 1997. "Higher order moment processing of laser Doppler perfusion signals." J Biomed Optic 2(4): 358-363.

Bergstrom, J., Furst, P., Noree, L. O. and Vinnars, E., 1974. "Intracellular free amino acid concentration in human muscle tissue." J Appl Physiol 36(6): 693-7.

Bowen, W. J., 1949. "The absorption spectra and extinction coefficients of myoglobin." J Biol Chem 179(1): 235-45.

de Mul, F. F. M., Koelink, M. H., Kok, M. L., Harmsma, P. J., Greve, J., Graaff, R. and Aarnoudse, J. G., 1995. "Laser-Doppler Velocimetry and Monte-Carlo Simulations on Models for Blood Perfusion in Tissue." Appl Optic 34(28): 6595-6611.

Fredriksson, I., Larsson, M. and Strömberg, T., 2006. "Absolute flow velocity components in laser Doppler flowmetry." Optical Diagnostics and Sensing VI, San Jose, CA, USA, SPIE.

Fredriksson, I., Fors, C. and Johansson, J., 2007. "Laser Doppler Flowmetry - a Theoretical Framework," Department of Biomedical Engineering, Linköping University.

Fredriksson, I., Larsson, M. and Strömberg, T., 2008a. "Optical microcirculatory skin model: assessed by Monte Carlo simulations paired with in vivo laser Doppler flowmetry." J Biomed Optic 13(1): 014015.

Fredriksson, I., Larsson, M. and Strömberg, T., 2008b. "Forced Detection Monte Carlo Algorithms for accelerated Blood Vessel image Simulations." J Biophoton, DOI 10.1002/jbio.200810048

Hamberg, L. M., Hunter, G. J., Kierstead, D., Lo, E. H., Gonzalez, R. G. and Wolf, G. L., 1996. "Measurement of cerebral blood volume with subtraction three-dimensional functional CT." Am J Neuroradiol 17(10): 1861-1869.

Jacques, S. L., 1998. Skin Optics, Oregon Medical Laser Center News. http://omlc.ogi.edu/news/jan98/skinoptics.html

Jakobsson, A. and Nilsson, G. E., 1993. "Prediction of sampling depth and photon pathlength in laser Doppler flowmetry." Med Biol Eng Comput 31(3): 301-7.

Jansson, E. and Sylvén, C., 1983. "Myoglobin concentration in single type I and type II muscle fibres in man." Histochemistry 78(1): 121-4.

Kienle, A. and Patterson, M. S., 1996. "Determination of the optical properties of turbid media from a single Monte Carlo simulation." Phys Med Biol 41(10): 2221-7.

Koelink, M. H., De Mul, F. F. M., Greve, J., Graaff, R., Dassel, A. C. M. and Aarnoudse, J. G., 1994. "Laser-Doppler Blood Flowmetry Using two Wavelengths - Monte-Carlo Simulations and Measurements." Appl Optic 33(16): 3549-3558.

Larsson, M., Steenbergen, W. and Strömberg, N. O. T., 2002. "Influence of optical properties and fiber separation on laser Doppler flowmetry." J Biomed Optic 7(2): 236-243.

Larsson, M. and Strömberg, N. O. T., 2006. "Toward a velocity-resolved microvascular blood flow measure by decomposition of the laser Doppler spectrum." J Biomed Opt 11(1): 014024.

Meglinsky, I. V. and Matcher, S. J., 2001. "Modelling the sampling volume for skin blood oxygenation measurements." Med Biol Eng Comput 39(1): 44-50.
Meier, R. R., Lee, J.-S. and Anderson, D. E., Jr., 1978. "Atmospheric scattering of middle UV radiation from an internal source." Appl Optic 17(20): 3216.
Millar, S. J., Moss, B. W. and Stevenson, M. H., 1996. "Some observations on the absorption spectra of various myoglobin derivatives found in meat." Meat Science 42(3): 277-288.
Nilsson, H. and Nilsson, G. E., 1998. "Monte Carlo simulations of light interaction with blood vessels in human skin in the red-wavelength region." Optical Diagnostics of Biological Fluids III, SPIE.
Rajan, V., Varghese, B., van Leeuwen, T. G. and Steenbergen, W., 2006. "Speckles in laser Doppler perfusion imaging." Optic Lett 31(4): 468-470.
Rajan, V., Varghese, B., Van Leeuwen, T. G. and Steenbergen, W., 2008. "Influence of tissue optical properties on laser Doppler perfusion imaging, accounting for photon penetration depth and the laser speckle phenomenon." J Biomed Optic 13(2).
Reynolds, L. O. and McCormick, N. J., 1980. "Approximate two-parameter phase function for light scattering." J Opt Soc Am 70(10): 1206-1212.
Ritz, J. P., Roggan, A., Isbert, C., Muller, G., Buhr, H. J. and Germer, C. T., 2001. "Optical properties of native and coagulated porcine liver tissue between 400 and 2400 nm." Laser Surg Med 29(3): 205-212.
Schenkman, K. A., Marble, D. R., Burns, D. H. and Feigl, E. O., 1999a. "Optical spectroscopic method for in vivo measurement of cardiac myoglobin oxygen saturation." Appl Spectros 53(3): 332-338.
Schenkman, K. A., Marble, D. R., Feigl, E. O. and Burns, D. H., 1999b. "Near-infrared spectroscopic measurement of myoglobin oxygen saturation in the presence of hemoglobin using partial least-squares analysis." Appl Spectros 53(3): 325-331.
Serov, A. and Lasser, T., 2006. "Full-field high-speed laser Doppler imaging system for blood-flow measurements."Advanced Biomedical and Clinical Diagnostic Systems IV, San Jose, CA, USA, SPIE.
Serov, A., Steenbergen, W. and de Mul, F., 2001. "Prediction of the photodetector signal generated by Doppler-induced speckle fluctuations: theory and some validations." J Opt Soc Am 18(3): 622-630.
Simpson, C. R., Kohl, M., Essenpreis, M. and Cope, M., 1998. "Near-infrared optical properties of ex vivo human skin and subcutaneous tissues measured using the Monte Carlo inversion technique." Phys Med Biol 43(9): 2465-78.
Taniguchi, H., Koyama, H., Masuyama, M., Mugitani, T., Koishi, Y., Tanaka, H., Hoshima, M., Miyata, K. and Takahashi, T., 1995. "Physiological hepatic imaging by positron emission tomography (PET)." Int Hepatol Comm 3: 101.
Tulevski, I. I., Ubbink, D. T. and Jacobs, M. J. H. M., 1999. "Red and green laser Doppler compared with capillary microscopy to assess skin microcirculation in the feet of healthy subjects." Microvasc Res 58(2): 83-88.
van der Zee, P., 1992. "Measurement and Modelling of the Optical Properties of Human Tissue in the Near Infrared." Department of Medical Physics and Bioengineering. London, University College London.
Yaroslavsky, A. N., Schulze, P. C., Yaroslavsky, I. V., Schober, R., Ulrich, F. and Schwarzmaier, H. J., 2002. "Optical properties of selected native and coagulated human brain tissues in vitro in the visible and near infrared spectral range." Phys Med Biol 47(12): 2059-2073.
Zijlstra, W. G., Buursma, A. and Assendelft, O. W. v., 2000. "Visible and near infrared absorption spectra of human and animal haemoglobin Determination and application." Utrecht, Boston, Köln, Tokyo, VSP.